Optical Review (2019) 26:247–261
https://doi.org/10.1007/s10043-019-00492-9

REGULAR PAPER

An efficient onboard compression method for multispectral images using distributed post-transform in the wavelet domain in conjunction with a fast spectral decorrelator

Jin Li[1] · Zilong Liu[2] · Shou-fu Tian[3]

Received: 1 September 2018 / Accepted: 27 December 2018 / Published online: 19 February 2019

Abstract
A remote sensing multispectral image compressor must be of low-complexity, high-robustness, and high-performance because it is usually located on a satellite platform where resources, such as power, memory, and processing capacity, are limited. Multispectral images having multiple bands are mainly compressed using compression algorithms based on three dimensional (3D) transforms, such as the 3D discrete wavelet transform, which exhibits satisfactory compression performance. However, the principal compression algorithm used for multispectral images having relatively a few bands is to encode each band independently, without considering the spectral redundancy between bands, which results in low compression performance. In this paper, an efficient compression method for multispectral images having a few bands is proposed, which is based on a distributed, improved post-transform in conjunction with a low-complexity, fast spectral decorrelator. First, a fast spectral transform and an improved post-transform having only a fast principal component analysis basis are used to generate the spectral and spatial sparse representation. Second, a distributed, improved bit plane encoding is integrated into the post-transform to remove the remaining spectral and spatial redundancy. Experimental results show that the proposed approach improves compression performance for test data in different performance measures: peak signal-to-noise ratio, mean structural similarity index, and visual information fidelity. Compared with current state-of-the-art compression techniques, the proposed method exhibits a performance improvement of 0.3–1.7 dB PSNR.

Keywords Remote sensing camera · Multispectral image · Compression · CCSDS · KLT/PCA · Post-transform · Wavelet

1 Introduction

With the development of imaging technology in space satellite optical cameras based on the multispectral time-delay-integration-charge-coupled-device (TDICCD), the requirements of the performance specifications, such as field of view (FOV), spatial resolution, time resolution, spectral resolution, radiometric resolution and wide swath, have been constantly improved in recent years [1–4]. At the same time, the number of TDICCDs which are used for splicing into long linear arrays is growing. The read speed rate of TDICCD and the quantization bits of an analog-to-digital convertor in a TDICCD video processor have also been improving. These factors have led to a dramatic increase in the total amount of digital image data of multispectral TDICCD cameras [5–7]. However, the storage capacities of satellite solid-state recording devices are limited and satellite downlink channel bandwidth is also restricted. The present storage devices and downlink technology have difficultly adapting the huge amount of data relating to multispectral TDICCD images. Therefore, the multispectral image data must be compressed when TDICCD cameras work in orbit.

Presently, the prevailing compression algorithms generally use a three dimensional (3D) transform technology to compress multispectral images [8]. The 3D transform-based compression approach of multispectral images usually has

✉ Zilong Liu
liuzl@nim.ac.cn

✉ Shou-fu Tian
sftian@cumt.edu.cn

[1] Electrical Engineering Division, Department of Engineering, University of Cambridge, Cambridge, UK

[2] Optic Division, National Institute of Metrology, Beijing 100029, China

[3] School of Mathematics, China University of Mining and Technology, Xuzhou 221116, People's Republic of China

an image transform stage, such as discrete cosine transform (DCT) [9], discrete wavelet transform (DWT) [10] and Karhunen–Loeve transform (KLT) [11]. The transform stage can remove spatial and spectral redundancies. Then, the transformed coefficients are encoded by entropy encoding algorithms, such as Embedded Zero-tree Wavelet [12], Embedded Block Coding with Optimization Truncation (EBCOT) [13], Set Partitioning in Hierarchical Trees (SPIHT) [14], Set Partitioned Embedded Block Coder (SPECK) [15], and Bit Plane Encoder (BPE) [16, 17]. The typical transform-based algorithms are JPEG2000, which are suitable for still images [18]. In the JPEG2000 algorithm, EBCOT technology is a very efficient approach to remove the redundancy between wavelet coefficients. The EBCOT technology enables JPEG2000 to have an excellent compression performance. However, it is too complex to be implemented in a space satellite TDICCD camera. Another typical transform-based algorithm is the Consultative Committee for Space Data Systems (CCSDS)—Image Data Compression (CCSDS-IDC) algorithm [19–23]. The CCSDS-IDC algorithm is mainly used in space application. The CCSDS-IDC algorithm contains two stages: (1) DWT; (2) BPE. The BPE is a zero tree encoder. It makes full use of the structures of spatiotemporal orientation trees in a bit plane. In other words, grandchildren coefficients also become not important when children coefficients are not important. The zero-tree characteristic causes the bit plane to have a large number of zero areas. Taking full advantage of these zero areas can improve coding efficiency. The CCSDS-IDC algorithm has the characteristics of progressive coding and fault-tolerant capability. In addition, BPE is low-complexity and occupies less storage capacity, which is suitable for the application of on-board cameras. However, the CCSDS-IDC method decreases the average peak signal to noise ratio (PSNR) by 2 dB compared with JPEG2000. In addition, CCSDS-IDC is only suitable for two dimensional (2D) images, which cannot exploit the spectral redundancy between 3D images. Realizing the needs of remote sensing imaging sensors capturing multiple spectral bands, the CCSDS standard committee [21] published the CCSDS 123.0-B-1: Lossless multispectral and hyperspectral image compression recommended standard [22] and CCSDS 122.1-B-1: spectral pre-processing transform for multispectral and hyperspectral image compression [23]. These two multispectral and hyper-spectral image compression standards could provide the references of onboard lossless, near-lossless, and lossy compression. The compression standard of multispectral and hyperspectral images may be extended by the CCSDS committee in future more effective compression.

Many compression methods of multispectral images have been proposed [24] for space optical imaging systems. In 2004, Enrico et al. proposed a new context-based adaptive lossless image coding method to implement the lossless and near-lossless compression for hyperspectral images [25]. In 2007, Enrico et al. proposed a distributed source coding technique for the lossless compression of hyperspectral images [26]. Didier et al. used Graphics Processing Units to implement a lossless hyperspectral data compression system for space applications [27]. These lossless compression algorithms of multispectral and hyperspectral images can provide the references for the lossy compression of multispectral and hyperspectral images from optical remote sensors. In 2013, Enrico et al. analysed the predictor of the predictive lossy compression paradigm [28]. This work outlines the directions for improvement of the algorithms, especially in the treatment of noisy channels, and investigates the use of appropriate statistical models for the entropy-coding stage. Kiely et al. proposed a 3D progressive wavelet-based compressor for hyperspectral images [29]. They used a 3D wavelet decomposition structure to exploit correlations in all three dimensions of hyperspectral data sets, while facilitating elimination of spectral ringing artefacts. Klimesh et al. analysed the spectral ringing artefacts in hyperspectral image data compression to improve the reconstructed band quality [30]. These multispectral and hyperspectral image compression methods can efficiently complete the compression mission for space optical imaging sensors with multiple spectral bands. They also can provide the reference for the future space compression standard of multispectral and hyperspectral image compression.

The compression methods outlined above are mainly used in multispectral and hyperspectral images that have multiple bands. However, for now, compression algorithms of multispectral images with relatively few spectral bands usually ignore the spectral redundancy. Each band is encoded independently, which causes the problem of low compression performance for remote sensing multispectral images with relatively few spectral bands. Achieving such a compressed multispectral image with a few bands remains a crucial but unsolved issue. In order to address this problem, two methods are proposed in our previous work. In [31], a one-dimensional (1D) DCT was used to exploit the spectral information, and a Tucker decomposition (TD) in spatial transform domain was used to remove residual spectral redundancies between bands and residual spatial redundancies intra bands. A deep coupling approach was also used to manage the TD processing. This method focused on removing spatial redundancies. In [32], a low-complexity removing spectral redundancy algorithm was investigated, while a traditional method using DWT and BPE was used to remove the spatial redundancies.

To address the low compression performance of remote sensing multispectral images which have relatively a few bands, this paper proposes an effective compression method for these images based on a fast KLT in conjunction with a distributed post-transform in the wavelet domain. This

is able to achieve good performance with moderate complexity, so as to adapt to the application requirements of new generation of high-resolution multispectral TDICCD cameras with wide FOV. The proposed method can also be used in space smart cameras [33] integrated with navigation devices [34–36], in space compressed imaging cameras for micro-satellites [37], and for space visual-tracking systems [38, 39].

The rest of this paper is organized as follows. Section 2 presents the architecture of the method. In Sect. 3, the experimental results are demonstrated. Section 4 concludes the paper.

2 Proposed compression method

2.1 Overall architecture

Multispectral images are divided into two categories: multispectral image having a few bands (MIHFB) and multispectral image having normal bands (MIHNB). The MIHFB usually has a high spatial resolution and a relatively low spectral resolution. In other words, the MIHFB has a high spatial correlation (i.e. spatial redundancy) between two adjacent pixels in a spectral band, while the spectral correlation between two adjacent bands is relatively low. On the contrary, the MIHNB usually has a high spectral resolution and a relatively low spatial resolution. Thus, the MIHNB has the high spectral correlation between two adjacent bands, while the spatial correlation between two adjacent pixels in a spectral band is relatively low. Based on the two different features of MIHFB and MIHNB, MIHFB usually requires a compression algorithm with the high-performance in the spatial decorrelation, while the spectral decorrelation is relatively low. MIHNB usually requires a compression algorithm with the high-performance in the spatial decorrelation, while the spectral decorrelation is relatively low. In this paper, we define images having a band number of below 10 as MIHFB, and those having a band number of above 10 as MIHNB. MIHFBs are obtained by a multispectral TDICCD, which is composed of several TDICCD arrays in parallel and produces several bands simultaneously (Fig. 1). The optics reflected and radiated by a ground object converges on the thin optical film of the TDICCD surface through the optical system. Each band TDICCD array captures optical energy to obtain the corresponding spectral band image. Each band image contains 1D spatial information of ground objects. At this point, a 1D spectral and 1D spatial image is obtained by this multispectral TDICCD camera. When the camera moves along push-broom direction, additional 1D spatial information of ground objects is obtained. Through iterations of this process, the multispectral TDICCD camera produces 3D images. The number of bands of multispectral image can be customized by the user. The imaging system in Fig. 1 uses four bands, a number widely used in multispectral imaging having a few bands.

In our previous work, compression approaches of panchromatic and multispectral images are thoroughly researched [16, 17, 19]. In this paper, a new compression method of multispectral images for remote sensing camera having comparatively few spectral bands is proposed. Four bands are used as an example to illustrate the proposed method. To balance computational complexity and compression performance of the MIHFB, an efficient scheme based on low-complexity fast KLT (FKLT) combined with improved post transform (PT) and Distributed Source Coding (DSC) integrated with CCSDS-IDC (DSC-CCSDS) is proposed for multispectral images having a few bands. This method integrates FKLT, improved post-transform in the wavelet domain, optimized CCSDS-IDC and distributed

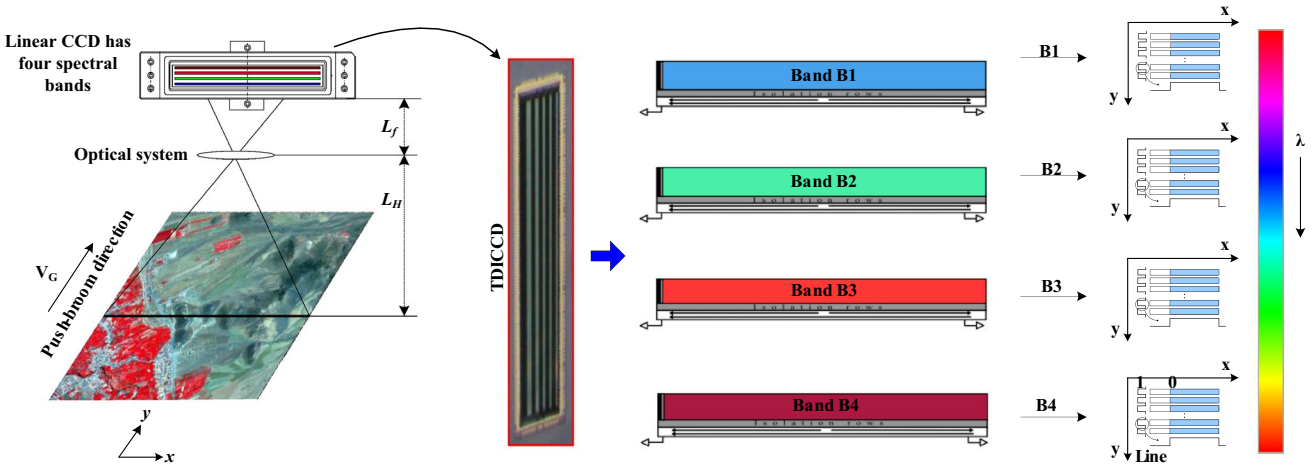

Fig. 1 Imaging principle of multispectral TDICCD with four bands, where L_f is the focal length of the camera, L_H is the orbital height

source coding to remove the spatial redundancy, spectral redundancy and bit information redundancy. The proposed compression encoder has than lower complexity than traditional ones, making it suitable for on-board camera applications.

Figure 2 shows the proposed compressor architecture of the MIHFB. The number of bands is four. First, all bands of multispectral images are transformed using a FKLT to remove the spectral redundancy. Then, a 3-level 9/7 lifting 2D DWT is attached to each principal component band to remove the intra-band spatial redundancy. Here, the lifting 2D DWT is a float form. In addition, an improved post-transform having only one fast principal component analysis (PCA) basis is attached to wavelet sub-bands of each band to exploit the remaining redundancy between adjacent wavelet coefficients intra-sub-band. Finally, an optimized DSC-CCSDS codec is used as an entropy coder to remove information redundancy and residual redundancy between the adjacent bands.

2.2 Fast KLT

KLT can be considered as an excellent method to remove the spectral redundancies between multispectral images [40–43]. However, the computation complexity of KLT is too high to be implemented in remote sensing applications. To lower the complexity, the following calculating strategy is adopted:

1. Spatial tiling

   The computation complexity of KLT is proportional to the size of each band [44, 45]. However, space camera has large wide-swath and high time resolution. The size of each band is very large. To accelerate computation speed, a tiling strategy is used in which a 3D multispectral image is spatially tiled. Each spatially tiled sub-block is considered as a new 3D multispectral image. The new 3D multispectral image is attached by KLT

2. Spectral band tiling

   In [45], the computational complexity of KLT is proportional to the number of bands in the multispectral images. A spectral band tiling strategy is used based on the idea of the clustering successive approximation method in [46–48], and [66]. Each spatially tiled sub-block, which has L spectral bands, is spectrally tiled to form several groups. Each two spectral bands are considered as a spectral tiled group. A KLT is attached to each spectral tiled group. Each spatially tiled sub-block is transformed by n level KLT. In first level transform, the L spectral bands can be spectrally tiled into $L/2$ groups. Each spectral tiled group includes two spectral bands and is transformed by KLT to form the first principal component spectral band and the second principal component spectral band. For each spatially tiled sub-block, the $L/2$ first principal component spectral bands and the $L/2$ s principal component spectral bands can be obtain in the first level transform. Since most of image energy is focused on the first principal component spectral bands, the redundancy between spectral tiled bands has been removed. Then, the $L/2$ first principal component spectral bands in the first level can be transformed by KLT at the second level. The transform approach in the second level is the same as the first. The transform approach at each level is the same until the n level transform is completed. Finally, the L principal component spectral bands can be obtained. When the number of spectral bands in one level is an odd number, the unpaired component exists. In this case, the unpaired component is directly forwarded to the next level. In other words, the unpaired components are seen as a principal component at successive levels.

3. Covariance matrix computation

   To reduce the computational complexity of KLT, a sub-sampling strategy is used to calculate the covariance matrix of the spectral tiled group, as in [42, 49]. In the sub-sampling strategy, 1% of the spectrum vectors are selected randomly to evaluate the covariance matrix, while the PSNR is not decreased. The complexity of the evaluation of the covariance matrix of full KLT is $\left(B_{\mathrm{KLT}}^2 M_{\mathrm{KLT}} N_{\mathrm{KLT}}\right)$, where B_{KLT} is the band number, and M_{KLT} and N_{KLT} are the size of each band in the horizontal and vertical direction. After the use of the sub-sampling strategy, the computational complexity of the covariance matrix is decreased to $\left(B_{\mathrm{KLT}}^2 M_{\mathrm{KLT}} N_{\mathrm{KLT}}/100\right)$.

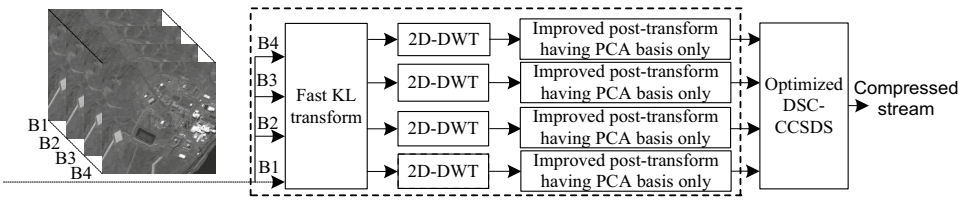

Fig. 2 The proposed coding architecture for MIHFBs

4. Eigenvalues and eigenvectors computation
   The Jacobi algorithm is used to implement the eigenvalue and eigenvector computations in the KLT process. In order to increase the calculation speed and to be easily realized by hardware, an optimized Jacobi algorithm is used based on the pipeline and parallel architecture detailed in [50]-[51].

5. Spectral transform computation
   Several lifting strategies of KLT are used to implement spectral transform computation, as given in [52–56]. According to the aforementioned tiling spectral bands, the associated lifting structure of spectral transform computation can be designed. The spectral transform is expressed as

$$G = V^T H = \begin{bmatrix} G_1 \\ G_2 \end{bmatrix} = V^T \begin{bmatrix} H_1 \\ H_2 \end{bmatrix}, \tag{1}$$

where V is eigenvector of the covariance matrix of H=[H_1, H_2]$^{\mathrm{T}}$. The covariance matrix of H is denoted as Cov(H), which can be expressed as:

$$\mathrm{Cov}(H) = \frac{1}{4} H^T H = \begin{bmatrix} \mathrm{cov}_{11} & \mathrm{cov}_{12} \\ \mathrm{cov}_{21} & \mathrm{cov}_{22} \end{bmatrix}. \tag{2}$$

V is expressed as

$$V^{\mathrm{T}} = \begin{bmatrix} v_{11} & v_{12} \\ v_{21} & v_{22} \end{bmatrix}. \tag{3}$$

The eigenvector is computed as:

$$v_{11} = v_{22} = \sqrt{\frac{1}{2} + \frac{(\mathrm{cov}_{11} - \mathrm{cov}_{22})}{2\eta}} = \sqrt{1 - {v_{21}}^2}, \tag{4}$$

$$v_{21} = -v_{12} = \frac{\mathrm{cov}_{12}}{|\mathrm{cov}_{12}|} \sqrt{\frac{1}{2} - \frac{\mathrm{cov}_{11} - \mathrm{cov}_{22}}{2\eta}}, \tag{5}$$

$$\eta = \sqrt{(\mathrm{cov}_{11} - \mathrm{cov}_{22})^2 + 4\mathrm{cov}_{12}\mathrm{cov}_{21}}. \tag{6}$$

Let $g = v_{21}$, V is expressed as

$$V = \begin{bmatrix} \sqrt{1-g^2} & -g \\ g & \sqrt{1-g^2} \end{bmatrix}. \tag{7}$$

Since Det (A) = 1 [57], V can be decomposed as:

$$V = \begin{bmatrix} t & -g \\ g & t \end{bmatrix} = \begin{bmatrix} 1 & 0 \\ f & 1 \end{bmatrix} \begin{bmatrix} 1 & -g \\ 0 & 1 \end{bmatrix} \begin{bmatrix} 1 & 0 \\ f & 1 \end{bmatrix}, \tag{8}$$

where $t = (1 - g^2)^{0.5}$ and $f = (t - 1)/-g$. Based on Eq. 8 the lifting structure of spectral transform computation is designed as shown in Fig. 3. The computation structure requires only nine operations and a conditional permutation.

2.3 Improved PT having only fast PCA basis

To implement post-transform [58, 59], each sub-band of all the high frequency sub-bands, such as LHi, HLi, HHi, $i = 1,2,\ldots,L$, is organized into several blocks. When the distance between wavelet coefficients is larger than 4 pixels, the correlation between coefficients is relatively weak [60]. Therefore, each block is composed of 4×4 wavelet coefficients. The post-transform compression idea is that wavelet coefficient blocks are further transformed on a one particular direction basis (such as Bandelet, DWT, DCT and PCA) in a dictionary. The post-transform key idea is that wavelet coefficient blocks perform transform on a one certain direction basis in a dictionary. A wavelet coefficient block is denoted by f, which is composed of 16 wavelet coefficients. f can also be considered as a vector with A ($A = 16$) elements in $\mathbb{R}^A$. Let D denote the post-transform dictionary, which is composed of multiple orthonormal bases of $\mathbb{R}^A$. Let S be the number of basis in D. Let B_b be an orthonormal basis function in $D = \{B_1, B_2, \ldots B_b\}$, where $b \in [1, S]$ is the basis index. The A vectors of the orthonormal basis B_b are expressed by ϕ_a^b with $a \in [1, A], B_b = \{\phi_a^b\}_{a(a=1)}^{bA}$. Let f^b be a post-transformed coefficients block. The post-transform can be expressed as:

$$f^b = \sum_{a=1}^{16} \langle f, \phi_a^b \rangle \cdot \phi_a^b, \tag{9}$$

where f is a wavelet coefficients block.

Each wavelet coefficient block is projected onto S bases in the post-transform dictionary. The S post-transformed block can be obtained. Therefore, a best post-transformed coefficient block needs to be selected from the S

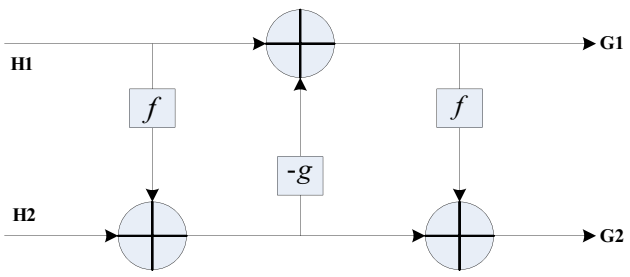

Fig. 3 Lifting structure of FKLT for MIHFBs

post-transformed blocked. In general, a minimum Rate-Distortion (RD) Lagrangian cost method is used to select a best post-transformed block, which can be expressed as:

$$L(f_q^b) = D(f_q^b) + \lambda \cdot R(f_q^b), \tag{10}$$

where f_q^b represents the quantized post-transformed coefficients, the quantization step is q, $\left(f_q^b\right)$ is the square error between f^b and f_q^b, λ is a Lagrangian multiplier, and $R\left(f_q^b\right)$ is the allocated bit-rate to encode f_q^b.

In our previous work [16, 17, 19] an improved post transform encoder was proposed. Some optimized strategies were used, such as a very simple dictionary which can be composed of the Hadamard transform (HT) and DCT basis, l_0 and l_1 norm for the best post-transform basis selection. Our previous work points out that PCA is the best post transform basis. However, PCA has very heavy computation complexity. It is not suitable for post-transform application. Because the fast strategy is utilized in computing KLT in the above section, the fast PCA is also implemented. So, the fast PCA as a post transform basis is used in this paper. The proposed encoder is shown in Fig. 4. The improved post-transform in the DWT domain is used to remove spatial redundancies. A fast PCA basis is adopted to further exploit the spatial redundancy within a wavelet-transform sub-band due to better sparse performance.

The post-transformed coefficients are encoded by the BPE encoder which is a zero tree encoder. However, the post-transform destroys the zero structure of wavelet coefficients. Each wavelet sub-band is performed by 4×4 post-transform. In one BPE block, the structure relationship between grandchildren and children coefficients is 2×2 children coefficients and 4×4 grandchildren. The post-transform block is 4×4. The process is expressed in Fig. 5.

If BPE builds the block structure as traditional wavelet spatiotemporal orientation trees, the 4×4 post-transform block of HL2, LH2 and HH2 consists of children coefficients in four orientation trees, and the 4×4 post-transform block of HL3, LH3 and HH3 consists of grandchildren coefficients in four orientation trees. The four orientation trees can be expressed as:

$$\mathrm{SOT}^a = \left\{C_0^a, C_1^a, C_2^a, G_0^a, G_1^a, G_2^a\right\}, \tag{11}$$

$$\mathrm{SOT}^b = \left\{C_0^b, C_1^b, C_2^b, G_0^b, G_1^b, G_2^b\right\}, \tag{12}$$

$$\mathrm{SOT}^c = \left\{C_0^c, C_1^c, C_2^c, G_0^c, G_1^c, G_2^c\right\}, \tag{13}$$

$$\mathrm{SOT}^d = \left\{C_0^d, C_1^d, C_2^d, G_0^d, G_1^d, G_2^d\right\}. \tag{14}$$

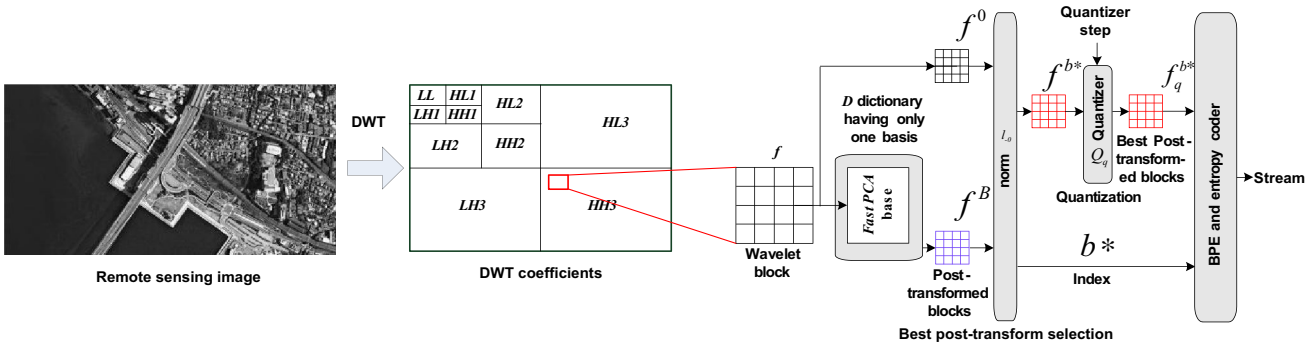

Fig. 4 Improved post-transform encoder for MIHFBs

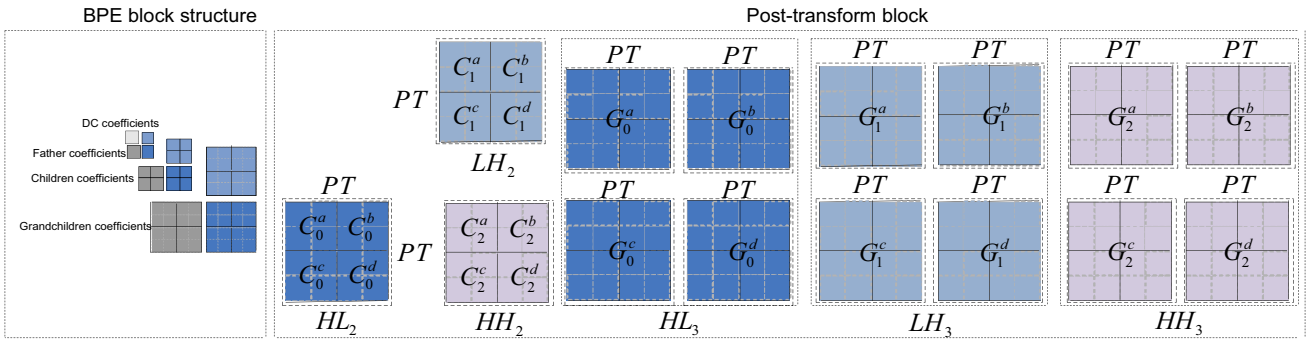

Fig. 5 Post-transform block structure

In BPE encoding, the four orientation trees are located in four separate encoding blocks of BPE. Grandchildren coefficients in each orientation tree are exactly one post-transform block. However, children coefficients are part of one post-transform block. This changes the original zero tree relationship between grandchildren and children coefficients. In this paper, a new BPE method is proposed to encode post-transform coefficients. To ensure the structures of spatiotemporal orientation trees, the structure of the traditional block is modified to four orientation trees representing one block, which is shown in Fig. 6.

The structure of the improved block includes three families. In each family, father coefficients are 4×4 coefficients, children coefficients are 4×4 coefficients, and grandchildren coefficients are 8×8 coefficients. Since grandchildren coefficients consist of a 4×4 post-transform block and a new family block is 8×8, the four post-transform coefficients of HL3, LH3 and HH3 in Fig. 5 are reordered. The energy of the reconstructed post-transform block can be concentrated in the top left corner, and low coefficients are concentrated in other parts. This can ensure the spatial orientation trees, which are beneficial, to be encoded by tran_B, $\text{tran}_{D,}$ tran_G, and $\text{tran}_{H_{i,j}}$. Finally, the four orientation trees are separated into four blocks, which are encoded by traditional BPE.

2.4 DSC-CCSDS strategy

The DSC method can obtain better compression performance of multispectral or hyperspectral images in the remote sensing application [61–67]. In our previous work in [19], a DSC strategy was combined with CCSDS-IDC to encode transformed coefficients. In this paper, the encoding process is optimized. The optimized coding process of the Slepian-Wolf bit plane encoding (SW-BPE) is summarized in Fig. 7.

3 Experimental results

3.1 Experiment setup

The proposed approach is tested and analyzed on a self-developed multispectral compression testing platform to verify the performance and feasibility of the proposed approach. The testing platform is shown in Fig. 8. The testing platform includes a multispectral image simulation source, a compression system, a compression and storage sever (CSS), a decoding unit, and a display system. The CSS can produce simulated multispectral images with three and four bands, which are transmitted to the image simulation source unit. The image simulation source unit adjusts the output line frequency, image size, and output time to simulate TDICCD output. The compression system compresses the received multispectral image or simulated multispectral image. The proposed method is implemented and tested on the compression system. The compression system uses Xilinx FPGA with a 32-bit MicroBlaze as the processor. The compressed streams are received and decoded by a decoding unit. In the decompression method, a deblocking filter is used to remove the block effects because the multispectral images are spatially titled before spectral transform in the proposed method. The reconstructed image is transmitted to the CSS.

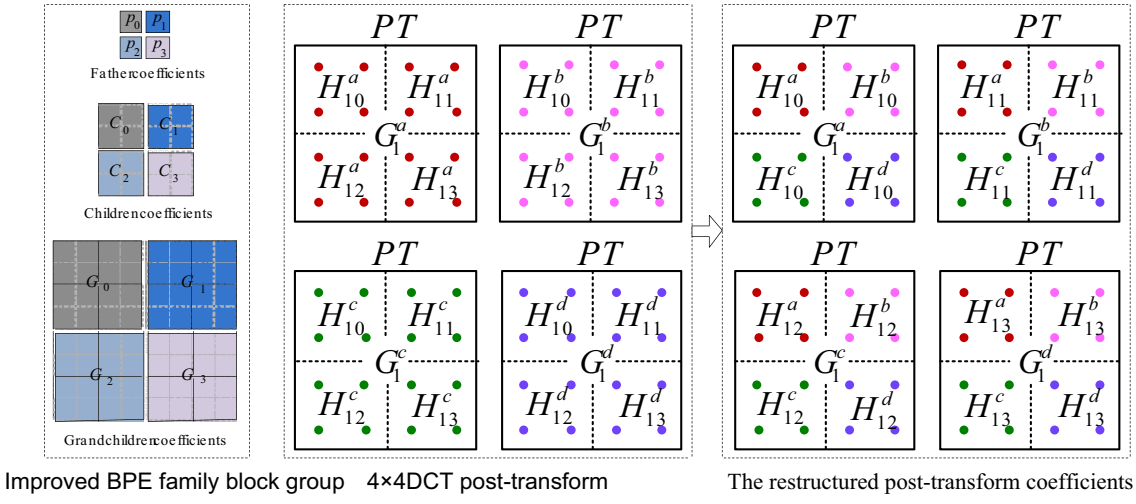

Fig. 6 Modifying the structure of the post-transform in the proposed method, the points represent the grandchildren coefficients in different directions

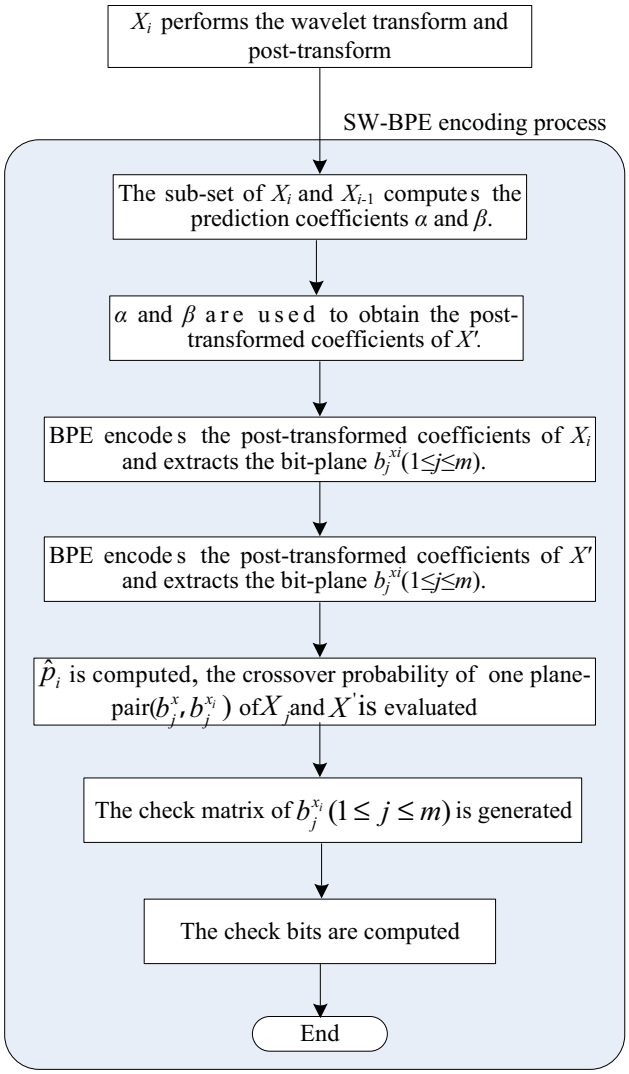

Fig. 7 DSC-CCSDS encoding flow in the proposed method

3.2 Compression experiments using image simulation sources

In order to verify the proposed compression scheme, the image simulation source unit produces several groups of multispectral remote sensing images that are transmitted to the compression system. They are rich in texture to verify validity and feasibility of the proposed approach. Each group has three bands, measuring radiation from the Earth filtered at wavelengths red, green, and blue. Each band of the remote sensing image is 8 bpp (bits per pixel). The FKLT is performed on each group of the multispectral remote sensing images. A three-level 9/7 Daubechies DWT and a fast PCA-based PT are performed on each band, and then the post-transformed coefficients are quantized. Figure 9 demonstrates the three reconstructed bands and the magnified sub-images. Each band is 491 × 491 pixels. The code rate of the key bands is 2.0 bpp. The PSNR of three bands can reach 51.56 dB, 50.48 dB, and 50.29 dB, respectively. After multispectral remote sensing images are transformed by the proposed FKLT-PT scheme, the bit-depth of transformed high frequency coefficients is 0–6 bit. The bit-depth of most of the coefficients is 0–4 bit. There are no large high-frequency coefficients. All reconstructed bands have no blocking effect, and high recovery-quality bands can be obtained.

In addition, the image simulation source unit produces several groups of Quickbird multispectral images to test the proposed algorithm. Each group has four bands, measuring radiation from the Earth filtered at wavelengths red, green, blue, and near-infrared. Each band in the remote sensing, multispectral images is 8 bpp. Figure 10 demonstrates the first reconstructed band and the magnified sub-image. From the magnified sub-image, the proposed algorithm can effectively preserve the edge information of the original multispectral images. Other groups can also obtain the same results.

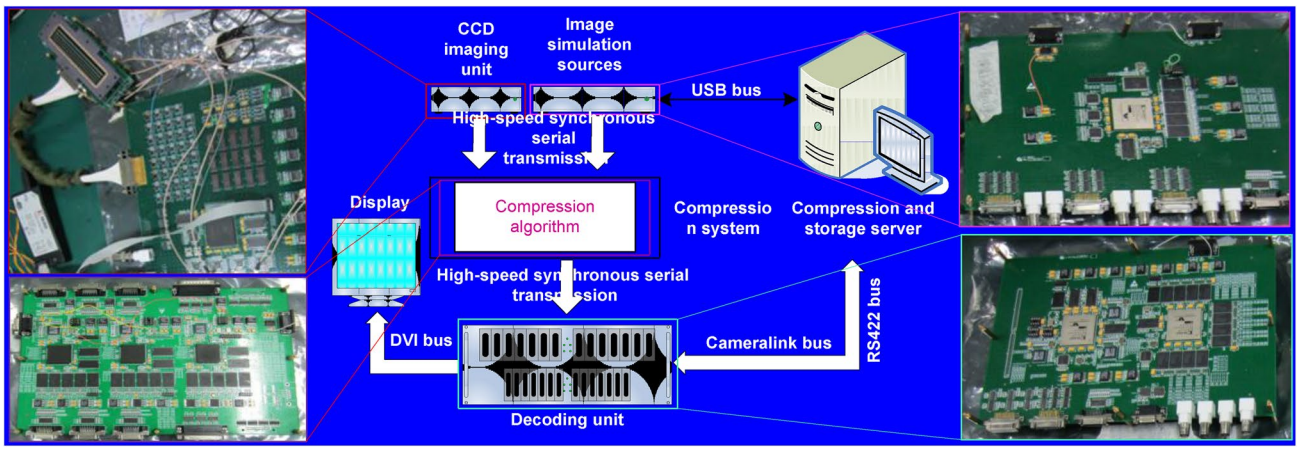

Fig. 8 Compression testing platform of the proposed method

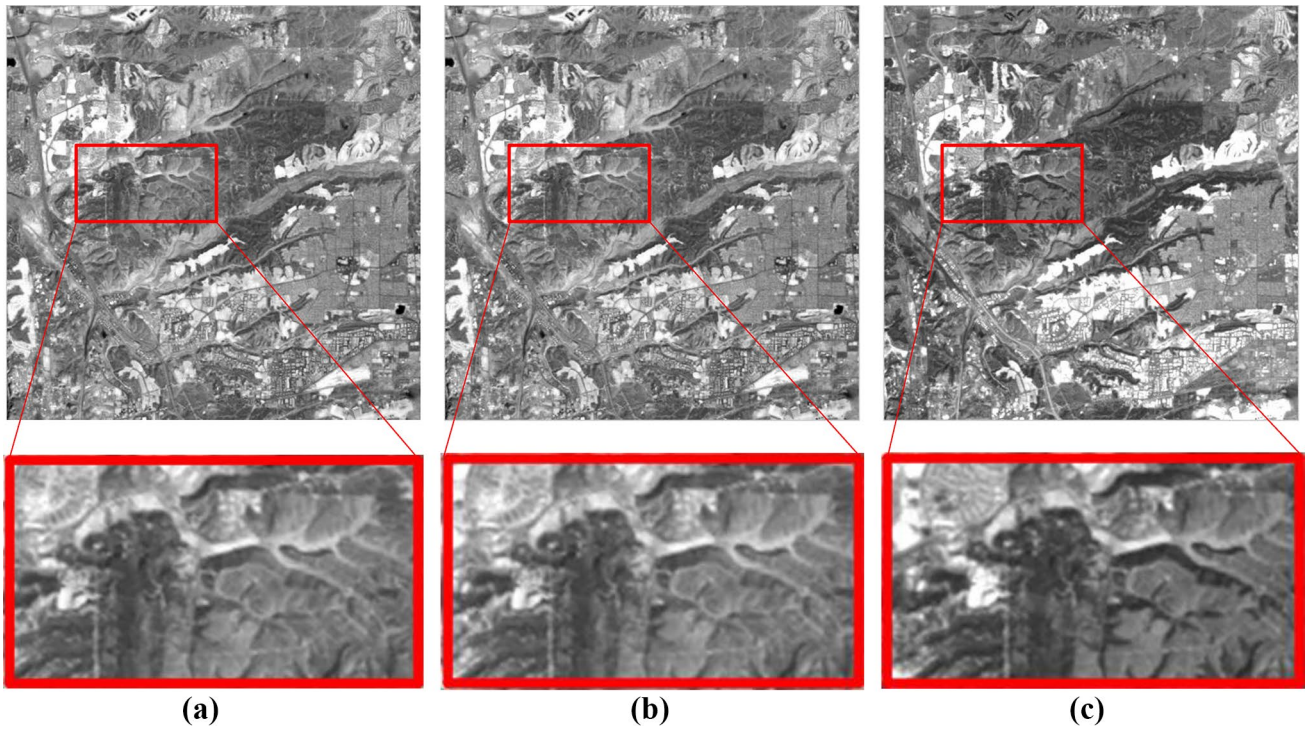

Fig. 9 Reconstructed multi-band images using the propose method at 2.0bpp, (a) reconstructed band1, (b) reconstructed band2, and (c) reconstructed band3

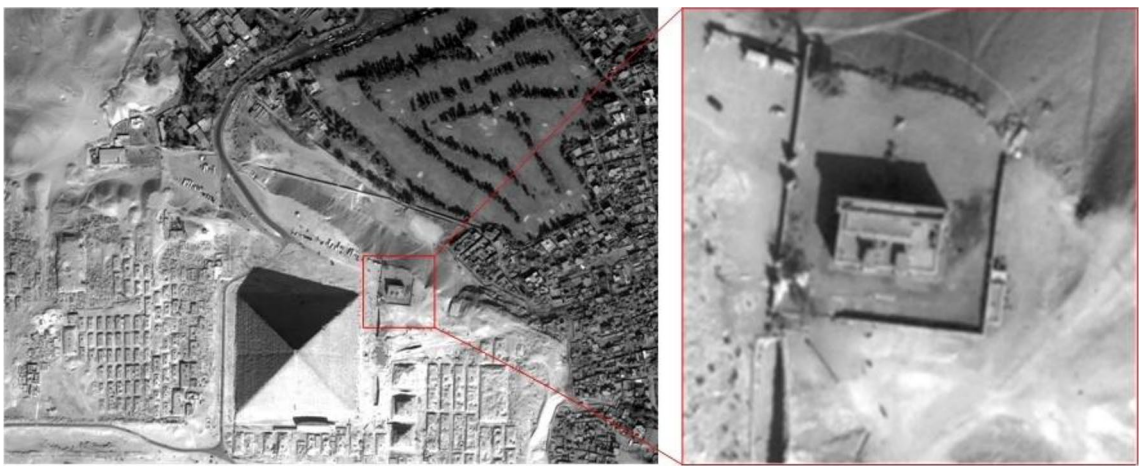

Fig. 10 Magnification of one segment of the first reconstructed band using the proposed method

Finally, a multi-spectral image is used to compare the compression experiments with two different methods. The captured images are compressed by the proposed algorithm and CCSDS-IDC approach at 0.5bpp. Figure 11 demonstrates the reconstructed image. Figure 11a, d show the original image and magnification of one segment S. Figures 11b, e show the reconstructed image of CCSDS-IDC. Figure 11c, f show the reconstructed image of the proposed method. As the figures show, the CCSDS-IDC method has the fuzzy phenomenon of a reconstructed image at low bit rates. The proposed method has no ringing effect and emerging distortion. Other bands depict the same results. Therefore, the proposed method works well for image compression while edge and outline information is substantially retained.

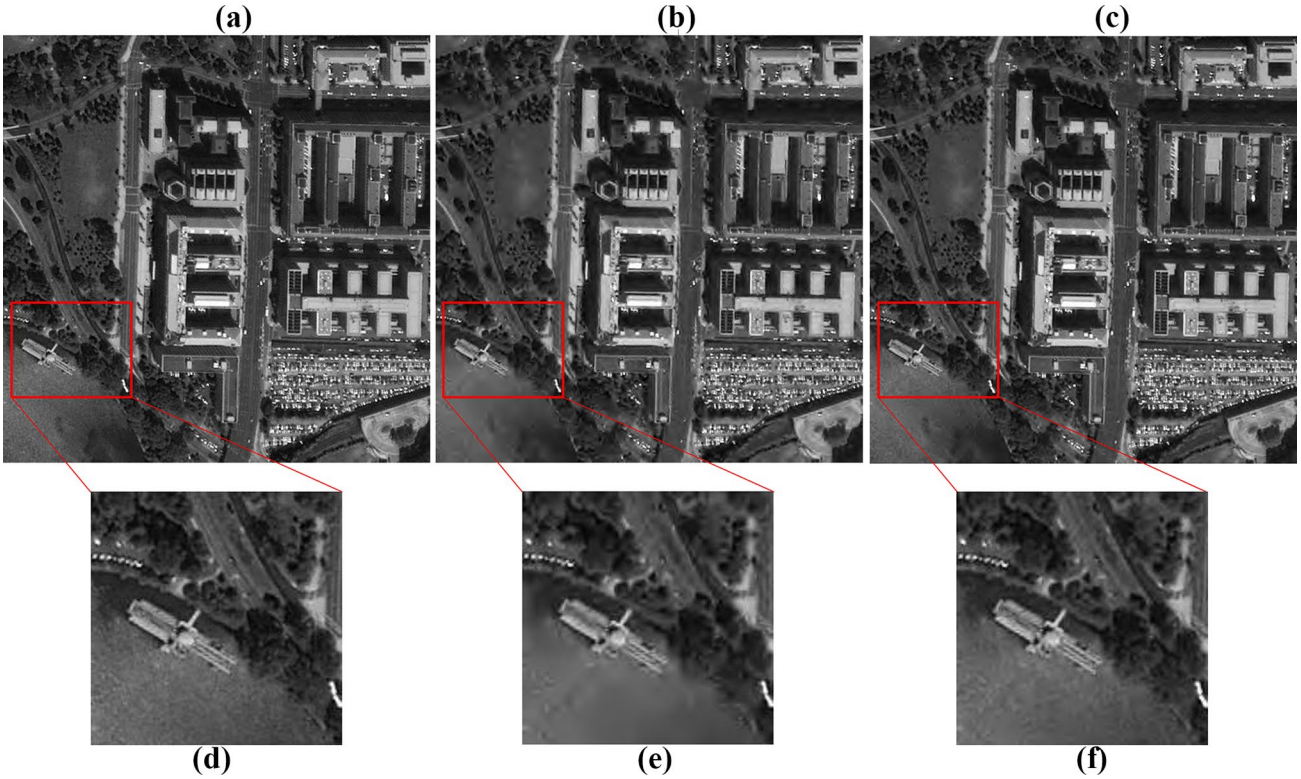

Fig. 11 Reconstructed multi-band images with different methods at 0.5 bpp, (a) The original first band, (b) Reconstructed band of S using CCSDS-IDC method, (c) Reconstructed band of S using the proposed method, (d) Magnification of one segment of the first band, (e) and (f) Magnification of two reconstructed images

3.3 Compression performance testing experiments

In order to objectively evaluate the performance of the proposed compression algorithm, the CSS injects multiple groups of AVIRIS uncalibrated multispectral images, including cities and buildings, into the image simulation sources to perform the compression experiment at different bit rates (BR). Each group is 512 pixel × 512pixel × 4, while the bit depth of every pixel is 8bit.

The compression bit rate is set to 0.25–2.0 bpp. The PSNR of the original and reconstructed multispectral images is used as the evaluation equation, which can be expressed as:

$$\mathrm{PSNR} = 20\log_{10}\left(\frac{2^{Q}-1}{\sqrt{\mathrm{MSE}}}\right)(\mathrm{dB}), \tag{15}$$

$$\mathrm{MSE} = \frac{1}{W\times H\times B}\sum_{k=0}^{B-1}\sum_{i=0}^{W-1}\sum_{j=0}^{H-1}\left(x_{i,j,k}-x'_{i,j,k}\right)^{2}, \tag{16}$$

where Q is the quantization bits of the original image sample, B is the band number of the multispectral image, W and H are the size of each band, $x_{i,j,k}$ and $x'_{i,j,k}$ denote the pixel value at (i, j,k) in original and reconstructed multispectral images, respectively.

First, the three groups (Hawaii, Jasper Ridge, and Lunar Lake,) of multispectral images with different textures are used as the testing images. Figure 12 shows the PSNR results of three group AVIRIS multispectral images using the proposed algorithm. In Fig. 12, the PSNR reaches above 40dB at 0.25–2 bpp. Second, the proposed algorithm on multiple groups for multispectral images is compared with PCA, SPIHT + 2D-DWT with KLT [68], SPECK + 2D-DWT [69] with KLT, and POT [70]. These four methods use the quantization method and entropy encoder of the JPEG2000 [71]. From Fig. 12, a compression algorithm is applied to two different multispectral images and two different PSNRs are obtained. We use 50 images from the testing image database are used to measure the corresponding PSNR. The average PSNR is considered as the PSNR of the corresponding method. The PSNR comparisons are demonstrated in Fig. 13a, b. Due to the full usage of FKLT and PT in the DWT domain, the proposed compression achieves a good compression performance. The proposed method can improve PSNR

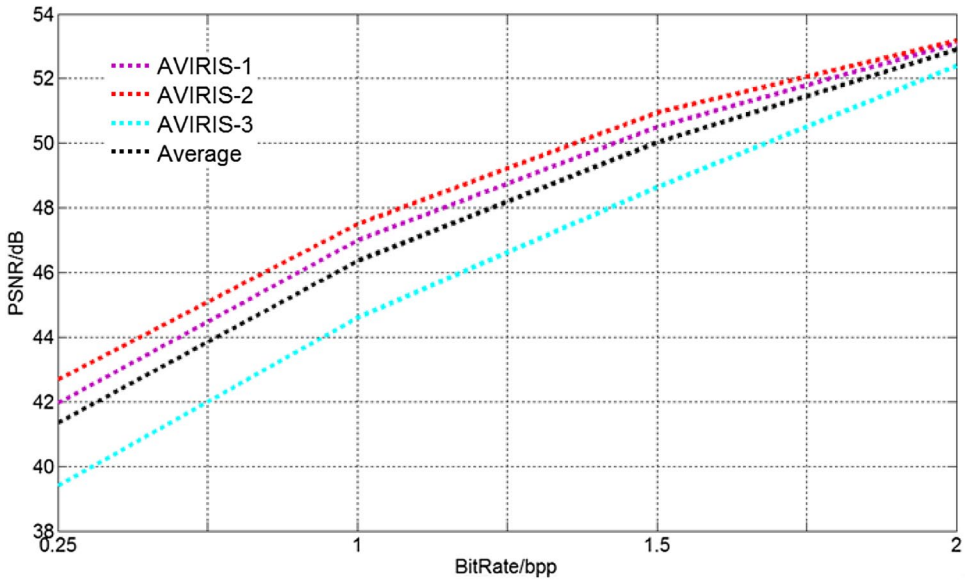

Fig. 12 Tested PSNR results with the proposed method on three group multispectral images

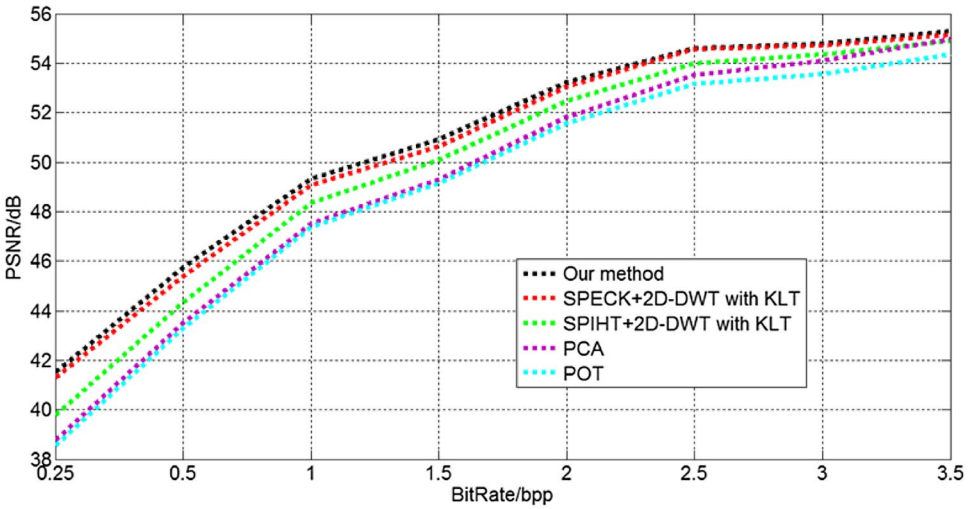

Fig. 13 PSNR comparison with traditional compression method at different bit rate

by 0.3–1.7 dB against SPIHT + 2D-DWT with KLT at 3.5–0.25 bpp.

Third, the proposed algorithm is compared with the CCSDS-IDC space compression standard method. As the same considerations with Fig. 13, the same compression algorithm has a different PSNR when a different multispectral image is used as the input. The same groups (50 images from the testing image database) of multispectral images are used as test input for compression algorithms. The average PSNR is considered as the PSNR of the corresponding method. Figure 14 shows the comparison of results for different compression algorithms. Since the compression method based on CCSDS-IDC without KLT does not remove the spectral redundancies, the compression performance is 2dB lower than CCSDS-IDC with KLT. In the proposed algorithm, FKLT and improved PT in the DWT domain are utilized to remove spatial and spectral redundancies, and DSC-CCSDS encodes the transform coefficients. Therefore, the PSNR of the proposed algorithm is 0.15–1.57 dB higher than CCSDS-IDC with KLT.

Finally, other evaluation parameters are used to analyze the compression performance of the proposed method. The CSS is injected by the same multispectral images. Other image quality assessment methods are performed by using the mean measure of structural similarity (MSSIM) [72] and visual information fidelity (VIF) [73]. The MSSIM and VIF are based on the hypothesis that the human visual system (HVS) is highly adopted for extracting structural information. The reference methods use the CCSDS-IDC method with KLT and the CCSDS-IDC method without KLT. The MSSIM and VIF values at different compressed ratios are shown in Table 1. Because several key technologies are used, such as the FKLT to remove spectral redundancy, and

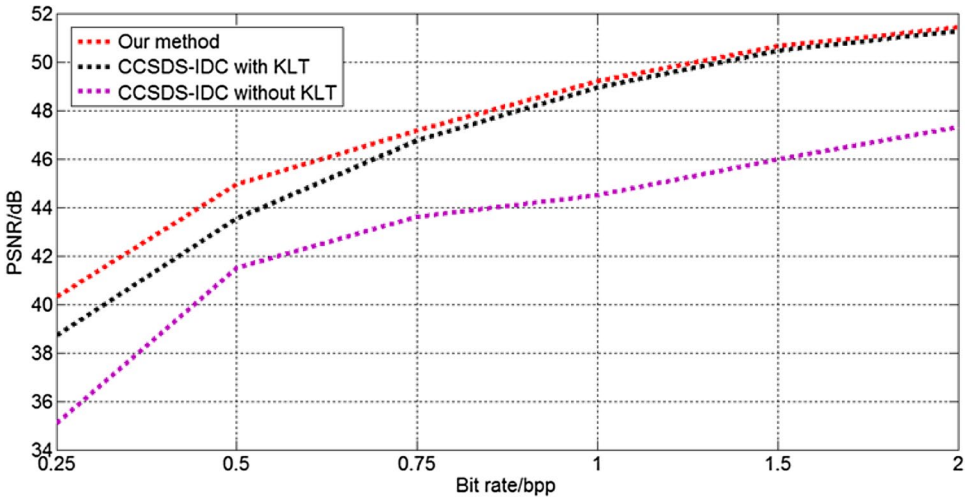

Fig. 14 Test result comparison (PSNR) with space compression standard at different bit rate

Table 1 MSSIM and VIF values at different compression ratio

Methods	Bitrate (bpp)	CCSDS-IDC (dB)	CCSDS-IDC-KLT (dB)	The proposed method (dB)
MSSIM	0.25	0.6848	0.7130	0.7466
	0.5	0.7727	0.8022	0.8169
	0.75	0.8217	0.8450	0.8608
	1.0	0.8540	0.8700	0.8807
	1.5	0.8703	0.8870	0.8996
	2.0	0.8853	0.8950	0.9044
VIF	0.25	0.4984	0.5183	0.5332
	0.5	0.5724	0.5911	0.6120
	0.75	0.6143	0.6325	0.6600
	1.0	0.6463	0.6713	0.6835
	1.5	0.6750	0.6895	0.7058
	2.0	0.6867	0.7013	0.7154

the improved post-transform method, the proposed method outperforms the traditional saliency-based methods.

3.4 Compression complexity analysis

In the proposed method, FKLT is performed on the spectral dimension to exploit spectral information. Let N be the band number of the multispectral image. The spectral band tiling is used based on multi-level decomposition to perform KLT. Let K be the number of sub-band unit (SBU) decomposed by spectral band tiling. For each SBU, $N=2$. Only a small sample of the image spatial locations is also used to compute the covariance matrix. Let ρ be Sub-sampling factor of the covariance matrix. The KLT calculation complexity of each SBU is shown in Table 2.

After applying FKLT, three-level 2D DWT is applied to the spatial bands. Let L be the decomposition level of 2D DWT. For the $I_1 \times I_2 \times I_3$ MIHFBs performing 2D-DWT, the calculation complexity is $\left(8NI_1I_2I_3(1-2^{-2L})\right)/6$. In the proposed method, a 9/7 2D-DWT is used to transform each band of MIHFBs. Three-level decomposition is performed. Therefore, the calculation complexity of the proposed method is $O(9I_1I_2I_3/7)$. After MIHFBs performing 2D DWT, The fast PCA is used based on pairwise orthogonal

Table 2 Calculation complexity of each SBU, M and L are the number of spatial locations

Step	Additions	Subtraction	Multiplication	Division	Trigonometry
BandMean	MLN	–	–	N	–
MeanSub	–	MLN	–	–	–
Covariance	$0.5\rho MLN(N+1)+MLN\rho$	N^2	$0.5\rho MLN(N+1)+0.5N(N+1)+N^2$	N^2+N	–
Eigen	$5(N-1)(N-2)\times(4+2N)$	$5(N-1)(N-2)\times(4+2N)$	$5(N-1)(N-2)\times(14+8N)$	$10(N-1)(N-2)$	$15(N-1)(N-2)$
Eigen × meansub	$MLN(N-1)$	–	MLN^2	–	–
Total	$MLN(1+1.5\rho 0.5\rho N)+5(N-1)$ $(N-2)\times(4+2N)$	$MLN+N^2+5(N-1)$ $(N-2)\times(4+2N)$	$MLN(N+0.5\rho N+0.5\rho)+(N+1)$ $(0.5N+1)+N^2+5(N-1)$ $(N-2)\times 14+8N$	$11N(N-1)+20$	$15(N-1)\times(N-2)$

transform to implement post-transform. Each post-transform block has 4×4 coefficients. Each block is taken as m vectors, and each vector has n components. The computational cost is $12mn+21n-8m-23$. After 2D-DWT coefficients performing post-transform, The BPE-DSC encoder adopts low-density parity-check codes (LDPC), of which the encoding complexity is $O(N^2)$. In this paper, quasi-cyclic LDPC are used for fast encoding. The encoding complexity is $0.17^2N^2 + O(N)$, where N is the code length. The basic operations are very simple, as they are sums in modulo-2 arithmetic.

In the following section, the calculation times of the proposed compression method are tested and analysed. TDICCD imaging mode is used to test the compression time of the proposed method. The line frequency of TDICCD is 0.86 KHz. The following compression time of the proposed algorithm is only used to perform the evaluations of compression time. The compression algorithm is not optimized for FPGA implementation. These evaluations are based on the lossy compression of remote sensing multispectral images with four bands. The size of each band is 3072×128. The compression time of the proposed algorithm is compared with that of other algorithms. Table 3 compares the results of the compression time for different compression algorithms. The processing time of the proposed algorithm is 0.049 us/sample, which indicates less time than other methods. The compression time of 128×3072 needs only 19.26 ms. According to the different principles of TDICCD imaging, the proposed compression algorithm can be optimized on an FPGA. An optimized implementation on a FPGA can take minimal time.

In addition, a compression method with a low memory requirement can be used in memory constrained environments. In order to evaluate the occupancy of the resources, the XC2V6000-6FF1152 FPGA is utilized to implement the proposed algorithm. These resources can implement the operation of the compression algorithm. The design language is VerilogHDL, the development platform is ISE8.2, and the synthesis tool is XST. Table 4 demonstrates the occupancy of resources of the proposed approach. From Table 3, the LUT occupies 81%, Slices occupy 76%, and BRAM occupies 86%. Various indicators are lower than 95%, which meet the requirement of our project.

Overall, the proposed algorithm in this paper achieves the excellent lossy compression performance and is very suitable for remote sensing multispectral images with a few bands.

Table 3 The results of complexity comparison

Methods	Times
The proposed method	0.049 us/sample
KTL [39]	0.102 us/sample
3DSPIHT [60]	0.062 us/sample
JPEG2000 [61]	0.181 us/sample

Table 4 The occupancy of resources

Resources	Utilization rate
Slices	27,481/33,792 (81%)
4 Input LUTs	51,792/67,584 (76%)
BRAM	124/144(86%)

4 Conclusion

In order to improve the compression performance of remote sensing MIHNBs, a low-complexity and efficient compression scheme has been proposed based on a distributed post-transform in the wavelet domain in conjunction with a fast spectral decorrelator. The new method uses a FKLT as the spectral decorrelator, followed by a post-transform having only fast PCA basis in the wavelet domain for the spatial decorrelation. In this algorithm, a new distributed BPE is proposed for encoding the post-transform coefficients. Multispectral images having different textures are used to verify validity and test compression performance of the proposed algorithm. Experimental results show that the proposed compression method offers the excellent compression performance based on different performance evaluation indices, such as PSNR, MSSIM and VIF. The experimental results are compared with various state-of-the-art compression techniques and exhibit a performance improvement of 0.3–1.7 dB PSNR over current techniques. The proposed algorithm is very suitable for MIHFBs and has the potential to compress MIHNBs and hyperspectral images. The next stage will be to optimize the proposed algorithm on an onboard hardware platform. We will also simplify the proposed algorithm, slightly compromising performance, to develop an on-board compressor.

Funding This work is supported by the Natural Science Foundation of China (Grant 61875180) and the National Key Research and Development Plan of China (Grant no. 2017YFF0205103).

References

1. Jia Zang, Y., Li, X., Xue, et al.: Multi-channel high-speed TDICCD image data acquisition and storage system. In: 2010 International conference on e-product e-service and e-entertainment (ICEEE 2010) (2010)
2. Zhi-le Wang, X., Zhuang, L., Zhang, Effect of image motion and vibration on image quality of TDICCD camera. Appl. Mech. Mater. 128–129, 584–588, (2012)

3. Hao Wang, Z., Yang, Y., Chen, et al.: A study on the influence of the satellite attitude accuracy on TDICCD imaging. In: Proceedings of the 2012 8th IEEE international symposium on instrumentation and control technology (ISICT 2012) pp. 219–23 (2012)
4. Xin, J.: Investigation on the MTF for the large-aperture long focal length TDICCD camera. In: 6th International symposium on advanced optical manufacturing and testing technologies (AOMATT)—advanced optical manufacturing technologies, proceedings of SPIE, vol 8416 (2012)
5. Li, J.: A highly reliable and super-speed optical fiber transmission for hyper-spectral SCMOS Camera. Opt. Int. J. Light Electron Opt. **127**(3), 1532–1545 (2016)
6. Li, J., Jin, L., Li, G., Zhang, K., Wang, W.: Application of ADV212 to the large field of view multi-spectral TDICCD space camera. Spectr. Spectr. Anal. **32**(6), 1700–1707 (2012)
7. Jin, L.X., Li, J., Hao, X.P.: Design of image transmission system for multi channel panchromatic TDICCD camera with large field of view. Appl. Mech. Mater. 380–384, 3758–3761 (2013)
8. Javidi, B., Do, C.M., Hong, S.-H., Nomura, T. Multi-spectral holographic three-dimensional image fusion using discrete wavelet transform. J. Display Technol. 2(4), 411–417 (2006)
9. Shayron Nichols, H., Kim, A.A., Humos, et al.: A performance evaluation on DCT and wavelet-based compression methods for remote sensing images based on image content. IEEE **30**(2), 358–363 (2009)
10. Aggoun, A.: Compression of 3D integral images using 3D wavelet transforms. J. Display Technol. **7**(11), 586–595 (2011)
11. Kanga, H.-H., Shinb, D.-H., Kima, E.-S.: Compression scheme of sub-images using Karhunen–Loeve transform in three-dimensional integral imaging. Optics Communications **281**(14), 3640–3647 (2008)
12. Shapiro, J.M.: An embedded wavelet hierarchical image coder. In: Proc. IEEE int. conf. acoustic, speech and signal processing, vol. 4, pp. 657–660 (1992)
13. Taubman, D.: High performance scalable image compression with EBCOT. IEEE Trans. Image Process. **9**(7), 1158–1170 (2000)
14. Said, A., Pearlman, W.A.: A new, fast, and efficient image codec based on set partitioning in hierarchical trees. IEEE Trans. Circuits Syst. Video Technol. 6(3), 243–250, (1996)
15. Pearlman, W.A., Islam, A., Nagaraj, N., Said, A.: Efficient, low-complexity image coding with a set-partitioning embedded block coder. IEEE Trans. Circuits Syst. Video Technol. 14(11), 1219–1235 (2004)
16. Li, J., Xing, F., Sun, T., You, Z.: Multiband CCD image compression for space camera with large field of view. J. Appl. Math. **347285**, 1–9 (2014)
17. Li, J., Xing, F., You, Z.: An efficient image compressor for charge coupled devices camera. Sci. World J. 2014, 840762, (2014)
18. Charrier, M., Cruz, D.S., Larsson, M.: JPEG 2000, the next millennium compression standard for still images. In: IEEE International conference on multimedia computing and systems, vol.1, pp. 131–132 (1999)
19. Li, J., Xing, F., Sun, T., et al.: Multispectral image compression based on DSC combined with CCSDS-IDC. Sci. World J. 2014, 738735 (2014)
20. Zabala, A., Vitulli, R., Pons, X.: Impact of CCSDS-IDC and JPEG 2000 compression on image quality and classification. J. Electr. Comput. Eng. 7611067, (2012)
21. Shah, D., Bera, K., Joshi, S.: Software implementation of CCSDS recommended hyperspectral lossless image compression. Int. J. Image Graph. Sign. Process. **7**(4), 35 (2015)
22. Lossless Multispectral & Hyperspectral Image Compression. Recommendation for Space Data System Standards, CCSDS 123.0-B-1. Blue Book. Issue 1. CCSDS, Washington (2012)
23. Spectral preprocessing transform for multispectral and hyperspectral image compression. Recommendation for Space Data System Standards, CCSDS 122.1-B-1. Blue Book. Issue 1. CCSDS, Washington D.C (2017)
24. Blanes, I., Magli, E., Serra-Sagrista, J.: A tutorial on image compression for optical space imaging systems. IEEE Geosci. Remote Sens. Mag. **2**(3), 8–26 (2014)
25. Magli, E., Olmo, G., Quacchio, E.: Optimized onboard lossless and near-lossless compression of hyperspectral data using CALIC. IEEE Geosci Remote Sens Lett, 1(1), 21–25 (2004)
26. Magli, E., Barni, M., Abrardo, A., Grangetto, M.: Distributed source coding techniques for lossless compression of hyperspectral images. EURASIP J. Adv. Signal Process. 2007(1):24 (2007)
27. Keymeulen, D., Aranki, N., Hopson, B., et al.: GPU lossless hyperspectral data compression system for space applications. In: Aerospace conference, IEEE. IEEE, 1–9 (2012)
28. Ricci, M., Magli, E.: Predictor analysis for onboard lossy predictive compression of multispectral and hyperspectral images. J. Appl. Remote Sens. 7(1), 074591 (2013)
29. Kiely, A., Klimesh, M., Xie, H., Aranki, N: ICER-3D: A progressive wavelet-based compressor for hyperspectral images, NASA Technical Report, Washington, DC. https://ntrs.nasa.gov/search.jsp?R=20060008608 (2005)
30. Klimesh, M., Kiely, A., Xie, H., et al.: Spectral ringing artifacts in hyperspectral image data compression. In: Hyperspectral Data Compression. Springer US, pp. 379–405 (2006)
31. Li, J., Xing, F., You, Z.: Compression of multispectral images with comparatively few bands using posttransform Tucker decomposition. Math. Probl. Eng. **296474**, 1–17 (2014)
32. Li, J., Liu, F., Liu, Z.: Efficient multi-bands image compression method for remote cameras. Chin. Opt. Lett. **2**, 018 (2017)
33. Li, J., et al.: High-accuracy self-calibration for smart, optical orbiting payloads integrated with attitude and position determination. Sensors **16**(8), 1176 (2016)
34. Guang, Z., Yuyang, L., Xingzi, B.: Conservative term constrained Kalman filter for autonomous orbit determination. IEEE Trans. Aerosp. Electr. Syst. 54(2), 783–793 (2017)
35. Ning, X., Wang, F., Jiancheng F.: An Implicit UKF for satellite stellar refraction navigation system. IEEE Trans. Aerosp. Electron. Syst. **53**(3), 1489–1503 (2017)
36. Roshanian, J., Yazdani, S., Ebrahimi, M.: Star identification based on euclidean distance transform, voronoi tessellation, and k-nearest neighbor classification. IEEE Trans. Aerosp. Electron. Syst. **52**(6), 2940–2949 (2016)
37. Li, J., Liu, Z.: Efficient compressed imaging method for a micro-satellite optical camera. Appl. Opt. **55**(28), 8070–8081 (2016)
38. Chair, Z., Varshney, P.K.: Optimal data fusion in multiple sensor detection systems. IEEE Trans. Aerosp. Electron. Syst. **1**, 98–101 (1986)
39. Xie, H., et al.: Adaptive visual servoing of UAVs using a virtual camera. IEEE Trans. Aerosp. Electron. Syst. **52**(5), 2529–2538 (2016)
40. Zhang, J., Fowler, J.E., Liu, G.: Lossy-to-lossless compression of hyperspectral imagery using three-dimensional TCE and an integer KLT. IEEE Geosci. Remote Sens. Lett. **5**(4), 814–818 (2008)
41. Saghri, J.A., Schroeder, S.: An adaptive two-stage KLT scheme for spectral decorrelation in hyperspectral bandwidth compression. In: Proc. SPIE, vol. 7443, pp. 744313 (2009)
42. Penna, B., Tillo, T., Magli, E., Olmo, G.: Transform coding techniques for lossy hyperspectral data compression. IEEE Trans Geosci. Remote Sens. **45**, 1408–1421 (2007)
43. Wang, L., Wu, J., Licheng, J., Shi, G.: Lossy-to-lossless hyperspectral image compression based on multilierless reversible integer TDLT/KLT. IEEE Geosci Remote Sens Lett. **6**(3), 587–591 (2009)

44. Egho, C., Vladimirova, T.: Hardware acceleration of the integer karhunen-loeve transform algorithm for satellite image compression. In: 2012 IEEE international geosciences and remote sensing symposium (IGARSS), pp. 4062–4065 (2012)
45. Egho, C., Vladimirova, T., Sweeting, M.N.: Acceleration of Karhunen–Loeve transform for system-on-chip platforms. In: Proceedings of the 2012 NASA/ESA conference on adaptive hardware and system (AHS 2012), pp. 272–279 (2012)
46. Blanes, I., Serra-Sagristà, J.: Cost and Scalability improvements to the Karhunen-Loêve transform for remote-sensing image coding. IEEE Trans. Geosci. Remote Sens. **48**(7), 2854–2863 (2010)
47. Yodchanan, W.: Lossless compression for 3-D MRI data using reversible KLT. In: 2008 international conference on audio, language and image processing, pp. 1560–15604 (2008)
48. Noor, N.R.M., Vladimirova, T.: Parallel implementation of lossless clustered integer KLT using OpenMP. In: Proceedings of the 2012 NASA/ESA conference on adaptive hardware and systems (AHS 2012), pp. 122–128 (2012)
49. Penna, B., Tillo, T., Magli, E., Olmo, G.: A new low complexity KLT for lossy hyperspectral data compression. In: IEEE international symposium on geosciences and remote sensing (IGARSS), pp. 3525–3528 (2006)
50. Bravo, I., Mazo, M., Lázaro, J.L., et al.: Novel HW architecture based on FPGAs oriented to solve the eigen problem. IEEE Trans. Very Large Scale Integr. (VLSI) Syst. **16**(12), 1722–1725 (2008)
51. Mei, W.Y., Ming, J., Shuai, L., et al.: An implementation of matrix eigenvalue decomposition with improved JACOBI algorithm. In: Proceedings 2010 first international conference on pervasive computing, signal processing and applications (PCSPA 2010), pp. 952–955 (2010)
52. Noor, N.R.M., Vladimirova, T.: Integer KLT design space exploration for hyperspectral satellite image compression. In: Proceedings 5th international conference, convergence and hybrid information technology, ICHIT, pp. 661–668, (2011)
53. Wang, L., Wu, J., Licheng, J., et al.: 3D medical image compression based on multiplierless low-complexity RKLT and shape-adaptive wavelet transform. In: Proceedings of the 2009 16th IEEE international conference on image processing (ICIP 2009), pp. 2521–2524 (2009)
54. Xin, L., Lei, G., Zhu-sheng, Y.: Lossless compression of hyperspectral imagery with reversible integer transform. Acta Photonica Sinica **36**, 1457–1462 (2007)
55. Hao, P., Shi, Q.: Matrix factorizations for reversible integer mapping. IEEE Trans. Signal Process. **49**(10), 2314–2324 (2001)
56. She, Y., Hao, P., Paker, Y.: Matrix factorizations for parallel integer transformation. IEEE Trans. Signal Process. **54**(12), 4675–4684 (2006)
57. Bruekers, F.A.M.L., van den Ad, Enden, W.M.: New networks for perfect inversion and perfect reconstruction. IEEE J. Sel. Areas Commun. **10**(1), 129–137 (1992)
58. Delaunay, X., et al.: Satellite image compression by directional decorrelation of wavelet coefficients. In: Acoustics, speech and signal processing, 2008. ICASSP 2008. IEEE international conference on IEEE (2008)
59. Delaunay, X., Chabert, M., Charvillat, V., et al.: Satellite image compression by concurrent representations of wavelet blocks. Annals of telecommunications-annales des telecommunications **67**(1–2), 71–80 (2012)
60. Delaunay, X., Chabert, M., Charvillat, V., Morin, G.: Satellite image compression by post-transform in the wavelet domain. Signal Process. pp. 599–610 (2010)
61. Stéphane, M., Frédéric: Analysis of low bit rate image transform coding. IEEE Trans. Signal Process. **46**(4), 1027–1042 (1998)
62. Le Pennec, E., Mallat, S.: Sparse Geometric image representations with bandelets. IEEE Trans. Image Process. 14(4), 423–438 (2005)
63. Zhang, J., Li, H., Chang Wen, C.: Distributed coding techniques for onboard lossless compression of multispectral images. In: Multimedia and expo, 2009. ICME 2009. IEEE international conference on. IEEE (2009)
64. Pan, X., Liu, R., Lv, X.: Low-complexity compression method for hyperspectral images based on distributed source coding. IEEE Geosci. Remote Sens. Lett. **9**(2), 224–227 (2012)
65. Wang, J., Liu, R., Zhao, H.: Low complexity DCT-based distributed source coding wits gray code for hyperspectral image. In: International conference on wireless communications and signal processing, pp. 1304–1308 (2009)
66. Abrardo, A., et al.: Error-resilient and low-complexity onboard lossless compression of hyperspectral images by means of distributed source coding. IEEE Trans. Geosci. Remote Sens. **48**(4), 1892–1904 (2010)
67. Myung, S., Yang, K., Kim, J.: Quasi-cyclic LDPC codes for fast encoding. IEEE Trans. Inf. Theory **51**(8), 2894–2901 (2005)
68. Khelifi, F., Bouridane, A., Kurugollu, F.: Joined spectral trees for scalable SPIHT-based multispectral image compression. IEEE Trans. Multimed. **10**(3), 316–329 (2008)
69. Gonzalez-Conejero, J., Bartrina-Rapesta, J., Serra-Sagrista, J.: JPEG2000 encoding of remote sensing multispectral images with no-data regions. IEEE Geosci. Remote Sens. Lett. **7**(2), 251–255 (2010)
70. Blanes, I., Serra-Sagristà, J.: Pairwise orthogonal transform for spectral image coding. IEEE Trans. Geosci. Remote Sens. **49**(3), 961–972 (2011)
71. Acharya, T., Tsai, P.S.: JPEG2000 standard for image compression: concepts, algorithms and VLSI architectures. Wiley, Hoboken (2005)
72. Wang, Z., Bovik, A., Sheikh, H., Simoncelli, E.: Image quality assessment: from error visibility structural similarity. IEEE Trans. Image Process. **13**(4), 600–612 (2004)
73. Sheikh, H., Bovik, A.: Image information and visual quality. IEEE Trans. Image Process. **15**(2), 430–444 (2006)